

Hybrid Quantum-Classical Graph Convolutional Network

Samuel Yen-Chi Chen,^{1,*} Tzu-Chieh Wei,^{2,†} Chao

Zhang,^{3,‡} Haiwang Yu,^{3,§} and Shinjae Yoo^{1,¶}

¹*Computational Science Initiative, Brookhaven National Laboratory, Upton, NY 11973, USA*

²*C. N. Yang Institute for Theoretical Physics and Department of Physics and Astronomy,
State University of New York at Stony Brook,
Stony Brook, NY 11794-3840, USA*

³*Physics Department, Brookhaven National Laboratory, Upton, NY 11973, USA*

(Dated: January 18, 2021)

Abstract

The high energy physics (HEP) community has a long history of dealing with large-scale datasets. To manage such voluminous data, classical machine learning and deep learning techniques have been employed to accelerate physics discovery. Recent advances in quantum machine learning (QML) have indicated the potential of applying these techniques in HEP. However, there are only limited results in QML applications currently available. In particular, the challenge of processing sparse data, common in HEP datasets, has not been extensively studied in QML models. This research provides a hybrid quantum-classical graph convolutional network (QGCNN) for learning HEP data. The proposed framework demonstrates an advantage over classical multilayer perceptron and convolutional neural networks in the aspect of number of parameters. Moreover, in terms of testing accuracy, the QGCNN shows comparable performance to a quantum convolutional neural network on the same HEP dataset while requiring less than 50% of the parameters. Based on numerical simulation results, studying the application of graph convolutional operations and other QML models may prove promising in advancing HEP research and other scientific fields.

* ychen@bnl.gov

† tzu-chieh.wei@stonybrook.edu

‡ czhang@bnl.gov

§ hyu@bnl.gov

¶ sjyoo@bnl.gov

I. INTRODUCTION

The high energy physics (HEP) community has a long tradition of processing large-scale datasets. Recent advances in machine learning (ML) and deep learning (DL) techniques have introduced many new valuable concepts and tools to augment HEP research [1–6]. For example, convolutional neural networks (CNN) have been transformative in streamlining analysis of large HEP datasets [7, 8]. Meanwhile, recent progress in graph convolutional neural networks (GCN) has helped manage the difficulties in processing sparse data [9–11], which is ubiquitous in HEP.

In parallel with the advancements in ML/DL, quantum computers, once cited as “impractical,” have been built by several companies [12–14]. In theory, quantum computing can solve certain problems that are unworkable using classical computers [15–18]. However, currently available quantum devices, the so-called *noisy intermediate-scale quantum* (NISQ) processors [19], are not capable of performing robust quantum computing with many numbers of qubits and large circuit depth due to the lack of quantum error correction. Thus, it is non-trivial to design a proper hybrid quantum-classical architecture that can harness the strength and scalability of both computing paradigms. For clarity, the term “hybrid” in this case represents using classical computers for optimization and quantum computers for certain complicated tasks.

Despite limits on the number of available qubits and circuit depth, numerous efforts have sought to design ML applications on NISQ devices. Indeed, a family of algorithms called *variational quantum algorithms* [20], which have been successful in calculating chemical ground states [20, 21], have achieved promising results in quantum machine learning (QML) [22–47]. Yet, certain problems have not been thoroughly studied under current QML techniques. For example, sparse data, which is common in scientific data, especially within the HEP community, generally is difficult for ML models, and it is unclear if current QML models can provide advantages in addressing this problem. In classical ML, one potential solution for dealing with sparse data is by incorporating graph convolutional operations in DL models. However, this has not been thoroughly investigated in the quantum domain.

This work presents a novel hybrid quantum-classical graph convolutional neural network (QGCNN) framework to demonstrate the quantum advantage over classical algorithms. Contributions stemming from this work include:

- Successfully demonstrate the hybrid model with graph convolutional operation and variational quantum circuits.
- Illustrate the superior performance in terms of testing accuracy over the classical multilayer perceptron (MLP) model and classical convolutional neural networks (CNN).
- Showcase the comparable performance in terms of testing accuracy to quantum convolutional neural networks (QCNN) on the same Deep Underground Neutrino Experiment (DUNE) dataset while requiring less than 50% of the model parameters.

In this paper, Section II introduces the HEP experimental data used in this work. In Section III, IV and V describe the new QGCNN architecture in detail. Section VI shows the QGCNN’s performance on the experimental data, followed by additional discussions in Section VII. Finally, Section VIII includes the concluding details.

II. TRAINING AND TESTING DATASET

This work uses the same simulated data as our team’s previous work in employing QCNN for HEP event classification [32]. The dataset is simulated for the DUNE experiment [48] with the Wire-Cell Toolkit [49] and LArSoft software [50]. By using the same dataset, we can compare our previous results to benchmark the performance of the new QGCNN algorithms. While details of the experiment and data simulation can be found in Ref. [32], we provide a brief description for completion (as follows).

The DUNE experiment is a long-baseline neutrino oscillation experiment to search for CP violation in the lepton sector, determine neutrino mass ordering, perform precision tests of the three-neutrino paradigm, detect supernova neutrino bursts, and search for nucleon decays beyond the Standard Model. The experiment currently is under construction and will start taking data in the next few years. The DUNE detector uses the Liquid Argon Time Projection Chamber (LArTPC) technology, which digitally records high-resolution images of particle activities [51–54] in the detector. The training and testing dataset used in this work is generated with a full detector simulation of DUNE [49, 50]. Single-particle images are generated by applying a realistic simulation of particle interaction, detector response, and digital signal processing [55]. Four different types of particles (μ^+ , e^- , π^+ , and p) are simulated. Figure 1 shows example images of simulated particles. The images have

a resolution of 480×600 pixels, where each pixel represents approximately 5×5 square millimeter spacially. Each particle's momentum is set such that the mean range of the particle is about 2 meters, so the classification is not sensitive to the image size. Because of differences in the mass, charge, and interaction types of the particles, the particles leave rather distinctive topological patterns in the recorded images as shown in Figure 1. Details about the underlining physics can be found in Ref. [32]. Similar to our QCNN work [32], the QGCNN algorithm seeks to classify the types of these different particles.

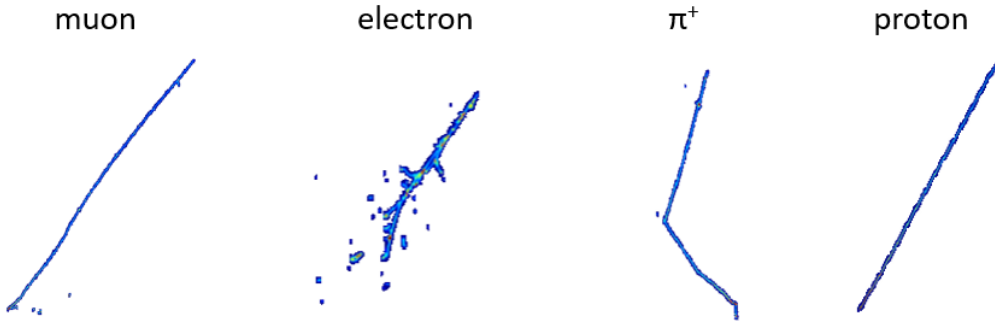


FIG. 1. Example images of simulated particle activities (μ^+ , e^- , π^+ , p) in a LArTPC detector. Colors in the images represent the intensity of the ionization energy loss recorded by each pixel.

III. GRAPH CONVOLUTION

A graph is an ordered pair $G = (V, E)$, where V is the set of nodes and E is the set of edges. The *adjacency matrix* A of an undirected graph \mathcal{G} with N nodes $\{u_1 \cdots u_N\}$ is an $N \times N$ matrix with the property that the element $A_{ij} = 1$ if there is an edge between node u_i and u_j and is 0 otherwise. The *normalized adjacency matrix* \mathcal{A} is defined to be

$$\mathcal{A} = D^{-1/2} A D^{-1/2}, \quad (1)$$

where $D = \text{diag}(d)$ for $d(i)$, the degree of node i . For an N -node graph G , the corresponding $D^{-1/2}$ is

$$D^{-1/2} = \begin{pmatrix} \frac{1}{\sqrt{d(1)}} & 0 & \cdots & 0 \\ 0 & \frac{1}{\sqrt{d(2)}} & \cdots & 0 \\ \vdots & \vdots & \ddots & \vdots \\ 0 & 0 & \cdots & \frac{1}{\sqrt{d(N)}} \end{pmatrix}. \quad (2)$$

Consider the graph with four nodes $\{n_1, n_2, n_3, n_4\}$ shown in Figure 2, and, on each node, there is a corresponding feature value f_i with $i = \{1, 2, 3, 4\}$. The feature vector X for this

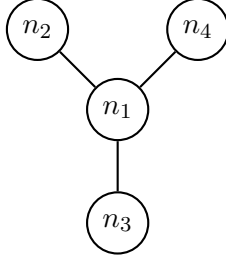


FIG. 2. **Example Graph.**

graph is

$$X = \begin{pmatrix} f_1 \\ f_2 \\ f_3 \\ f_4 \end{pmatrix}. \quad (3)$$

The adjacency matrix A for this graph is

$$A = \begin{pmatrix} 0 & 1 & 1 & 1 \\ 1 & 0 & 0 & 0 \\ 1 & 0 & 0 & 0 \\ 1 & 0 & 0 & 0 \end{pmatrix}. \quad (4)$$

The *graph convolution* operation here is the matrix multiplication AX :

$$AX = \begin{pmatrix} 0 & 1 & 1 & 1 \\ 1 & 0 & 0 & 0 \\ 1 & 0 & 0 & 0 \\ 1 & 0 & 0 & 0 \end{pmatrix} \begin{pmatrix} f_1 \\ f_2 \\ f_3 \\ f_4 \end{pmatrix} = \begin{pmatrix} f_2 + f_3 + f_4 \\ f_1 \\ f_1 \\ f_1 \end{pmatrix}. \quad (5)$$

In this example graph, the features of neighboring nodes aggregate together. When considering numerical computation, it is better to use the normalized adjacency matrix to avoid numerical instability (e.g., exploding values). In addition, we may want to modify the A to $\hat{A} = A + I$ in order to keep their individual features. This is equivalent to adding a *loop* for each node (Figure 3), Now, the adjacency matrix A becomes \hat{A} , which is

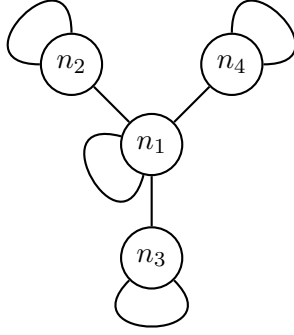


FIG. 3. **Example Graph with Self Loop.**

$$\hat{A} = A + I = \begin{pmatrix} 1 & 1 & 1 & 1 \\ 1 & 1 & 0 & 0 \\ 1 & 0 & 1 & 0 \\ 1 & 0 & 0 & 1 \end{pmatrix}. \quad (6)$$

Therefore, the aggregation operation is

$$\hat{A}X = \begin{pmatrix} 1 & 1 & 1 & 1 \\ 1 & 1 & 0 & 0 \\ 1 & 0 & 1 & 0 \\ 1 & 0 & 0 & 1 \end{pmatrix} \begin{pmatrix} f_1 \\ f_2 \\ f_3 \\ f_4 \end{pmatrix} = \begin{pmatrix} f_1 + f_2 + f_3 + f_4 \\ f_1 + f_2 \\ f_1 + f_3 \\ f_1 + f_4 \end{pmatrix}. \quad (7)$$

Consider an image with the size of $N \times N$. It can be viewed as a graph with N^2 nodes. Such a graph is *regular* because all nodes (pixels) of the graph are connected to each other in exactly the same manner. We define the adjacency matrix for an image based on the intuition that nearby nodes (or pixels) should have stronger relationships, while distant ones should have relatively weak relationships. For example, in a natural image, neighboring pixels are highly possible in the same object or architecture. The adjacency matrix A for this $N \times N$ image has the dimension $N^2 \times N^2$. Each element of A is calculated according to:

$$A_{ij} = \exp \left[\frac{-d_{ij}}{\sigma^2} \right], \quad (8)$$

where d_{ij} represents the Euclidean distance for the node pair (x_i, y_i) and (x_j, y_j) with the value $d_{ij} = \sqrt{(x_i - x_j)^2 + (y_i - y_j)^2}$. The parameter σ is the Gaussian scale. In this experiment, the value for σ is $0.05 \times \pi$.

For a 32×32 image, we can easily calculate the 1024×1024 dimension matrix A , and we can present this matrix as shown in Figure 4. We observe that the matrix values are much

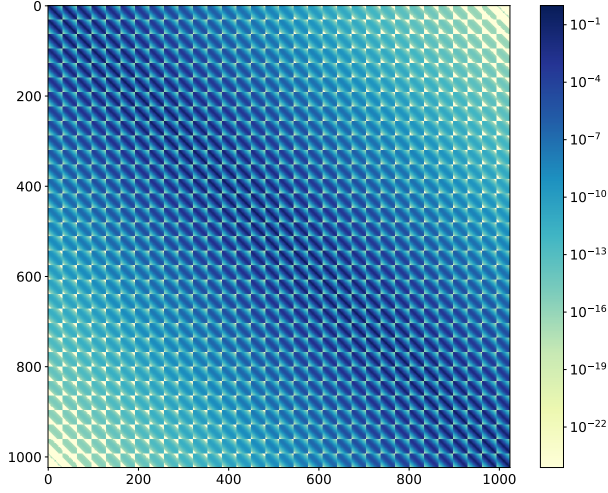


FIG. 4. **Adjacency matrix A for the 32×32 image.**

higher in the diagonal regions, corresponding to the fact that these points represent the node distances between nearby graph nodes. Here, we consider an example from the training set. In Figure 5, we demonstrate the effects of adjacency matrix A (defined in Equation 8) on the input image X from the DUNE-simulated dataset. The original X is rather sparse, making it difficult for QML models to classify. The situation worsens when encoding the image with amplitude encoding (described in Section IV A) as the vector normalization procedure causes significant information loss.

IV. VARIATIONAL QUANTUM CIRCUITS

Variational quantum circuits (VQC) are a special kind of circuit with parameters that are adjustable via optimization procedures developed by the classical ML community. This family of algorithms was first developed to calculate chemical ground states [21] and has been widely used [20]. VQCs also are known as “quantum neural networks,” or QNN, when applied in the ML field. Recent results have demonstrated that VQCs are more expressive than classical neural networks [56–59] with respect to the number of parameters or learning speed. Recent advances in VQC have demonstrated various applications in QML. For example, VQC has shown to be successful in the task of classification [22–30, 32, 60, 61],

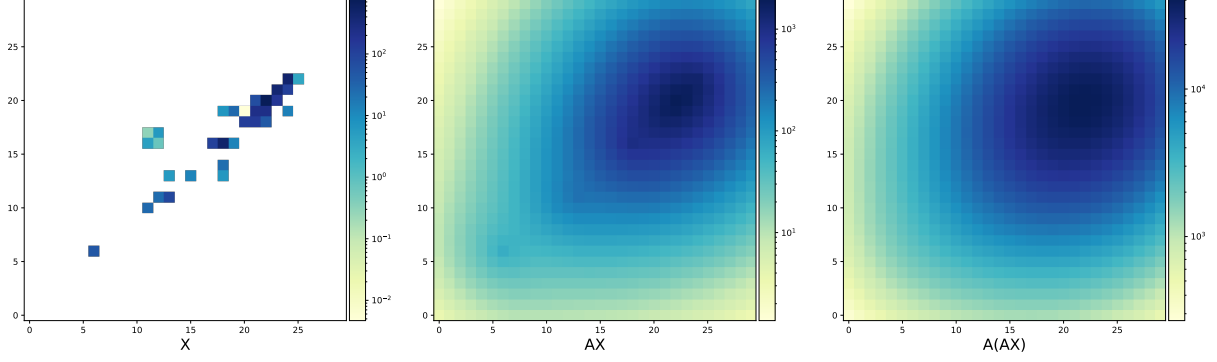


FIG. 5. **Examples of graph convolution on the DUNE data.** An example image from the DUNE dataset used in this study. The original image X is first flattened and multiplied by the adjacency matrix A . The transformed vector AX then is reshaped to the original image format. This depicts the result of AX and A^2X .

function approximation [31, 33, 60], generative ML [34–38], metric learning [39, 40], deep reinforcement learning [41–45], sequential learning [31, 46], and speech recognition [47]. For a VQC-based model to process classical data, it must first encode the classical data into a quantum state. A general N -qubit quantum state can be represented as:

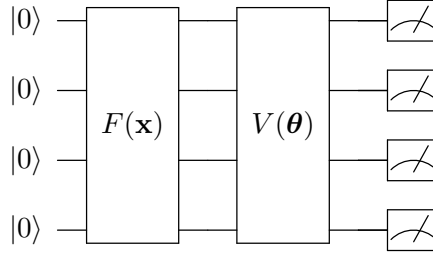


FIG. 6. **General structure for the variational quantum circuit.** The $F(\mathbf{x})$ is the quantum operation for encoding the classical data into the quantum state and $V(\boldsymbol{\theta})$ is the VQC block with the adjustable parameters $\boldsymbol{\theta}$. After the quantum operation, the quantum state is *measured* to retrieve classical numbers for additional processing. The additional processing may be a classical neural network or another variational quantum circuit.

$$|\psi\rangle = \sum_{(q_1, q_2, \dots, q_N) \in \{0,1\}^N} c_{q_1, \dots, q_N} |q_1\rangle \otimes |q_2\rangle \otimes |q_3\rangle \otimes \dots \otimes |q_N\rangle, \quad (9)$$

where $c_{q_1, \dots, q_N} \in \mathbb{C}$ is the *amplitude* of each quantum state and $q_i \in \{0, 1\}$. The square of the amplitude c_{q_1, \dots, q_N} represents the *probability* of measurement with the post-measurement

state in $|q_1\rangle \otimes |q_2\rangle \otimes |q_3\rangle \otimes \dots \otimes |q_N\rangle$, and the total probability should sum to unity, i.e.,

$$\sum_{(q_1, q_2, \dots, q_N) \in \{0,1\}^N} ||c_{q_1, \dots, q_N}||^2 = 1. \quad (10)$$

There are several different kinds of encoding methods that provide distinct quantum advantages with varying difficulties in the hardware implementation [62, 63]. Several recent advances suggest that the encoding operation itself can be learned from the dataset [39, 40]. The following sections introduce the two encoding schemes used in this work: *amplitude encoding* and *variational encoding*.

A. Amplitude Encoding

In the first VQC block, we employ *amplitude encoding* to reduce the number of qubits and circuit parameters. Here, we have a classical vector in the form of $(\alpha_0 \cdots \alpha_{2^n-1})$. The aim is to encode it into an n -qubit quantum state $|\Psi\rangle = \alpha_0 |00 \cdots 0\rangle + \cdots + \alpha_{2^n-1} |11 \cdots 1\rangle$, where the $\alpha_i \in \mathbb{R}$ and the vector $(\alpha_0 \cdots \alpha_{2^n-1})$ is a normalized vector (summed to unity). The details about this encoding method are introduced in the work of [64] and also can be found in the textbook [62]. The main reason to choose this encoding scheme is to minimize the number of qubits used, thereby reducing the number of circuit parameters. For example, given a vector with size N , it can be represented with a $\log_2(N)$ -qubit system with amplitude encoding. In this work, we consider the input vector with dimension $N = 32 \times 32 = 1024$ and n -qubit system with $n = 10$.

B. Variational Encoding

In the second VQC block, we employ *variational encoding*, where the input values are used as the quantum rotation angles. In variational encoding, there is a predefined sequence of single-qubit rotation gates for each qubit. A single-qubit gate with rotation along the j -axis by angle θ is given by

$$R_j(\theta) = e^{-i\theta\sigma_j/2} = \cos \frac{\theta}{2} I - i \sin \frac{\theta}{2} \sigma_j, \quad (11)$$

where I is the identity matrix and σ_j is the Pauli matrix with $j = x, y, z$. The *rotation angles* θ are calculated from the input values. In this study, we choose R_y and R_z to encode

the classical data with the rotation angles $\arctan(x)$ and $\arctan(x^2)$, respectively. Given an n -dimensional vector $\mathbf{x} = (x_1, x_2, \dots, x_n)$ to be encoded in an n -qubit circuit, the encoding operation can be written as

$$U(\mathbf{x}) = R_z(\arctan(x_1^2))R_y(\arctan(x_1)) \otimes \dots \otimes R_z(\arctan(x_n^2))R_y(\arctan(x_n)). \quad (12)$$

The circuit of this encoding is presented in Figure 9.

C. Optimization of Quantum Circuits

For gradient-based optimization to work, we employ the *parameter-shift* rule [65, 66] to calculate the gradients of quantum functions. This method has been highly successful in VQC-based QML tasks [25, 29, 31, 32, 41, 60, 66]. Given the knowledge of calculating the observable \hat{P} of a quantum function,

$$f(x; \theta_i) = \langle 0 | U_0^\dagger(x) U_i^\dagger(\theta_i) \hat{P} U_i(\theta_i) U_0(x) | 0 \rangle = \langle x | U_i^\dagger(\theta_i) \hat{P} U_i(\theta_i) | x \rangle, \quad (13)$$

where x is the classical input value (e.g. from input image array or post-measurement values of another quantum circuit) to the quantum circuit; $U_0(x)$ is the state preparation circuit to transform or encode the classical value x into a quantum state; i is the index of circuit parameter for which the gradient is to be evaluated; and $U_i(\theta_i)$ represents the single-qubit rotation generated by the Pauli operators X, Y , and Z . It has been shown in the work [60] that the gradient of this quantum function f with respect to the parameter θ_i is

$$\nabla_{\theta_i} f(x; \theta_i) = \frac{1}{2} \left[f\left(x; \theta_i + \frac{\pi}{2}\right) - f\left(x; \theta_i - \frac{\pi}{2}\right) \right]. \quad (14)$$

With the knowledge of calculating the quantum function gradients, it becomes straightforward to employ a variety of optimization algorithms developed by the classical ML community [67] and to train the whole hybrid architecture in an end-to-end fashion. In this work, the optimizer is chosen to be the RMSProp [68], which is a variant of gradient-descent method with the feature of adaptive learning rate. The circuit parameters θ are updated according to:

$$E[g^2]_t = \alpha E[g^2]_{t-1} + (1 - \alpha) g_t^2, \quad (15a)$$

$$\theta_{t+1} = \theta_t - \frac{\eta}{\sqrt{E[g^2]_t} + \epsilon} g_t, \quad (15b)$$

where g_t is the gradient at step t and $E[g^2]_t$ is the weighted moving average of the squared gradient with $E[g^2]_{t=0} = g_0^2$. The hyperparameters used in this work are: learning rate $\eta = 0.01$, smoothing constant $\alpha = 0.99$, and $\epsilon = 10^{-8}$.

V. GRAPH CONVOLUTION AND VQC

There are three major components in the proposed framework: 1) graph convolution, 2) VQC, and 3) classical post-processing. First, the original input image X with the dimension $N \times N$ will be flattened into a one-dimensional vector, and the adjacency matrix A , which is defined in Equation 8, will operate on it via matrix multiplication n times, which is set to be $n = 2$ in this work. Then, the aggregated vector $A^n X$ will be encoded into a quantum state via amplitude encoding described in Section IV A to maximally reduce the number of qubits used. The encoded quantum state then will go through several variational operations. Concretely, there are two VQCs separated by a tanh activation function. The first VQC (in Figure 8) is responsible for the amplitude encoding process and variational operations. The Pauli- Z expectation values from the first VQC subsequently are encoded via the variational encoding method (described in Section IV) into the second VQC (see Figure 9) and undergo variational operations. Finally, the measured expectation values from the final VQC block (the second VQC in this study) are processed with a single-layer classical neural network to output the logits for each class. For a schematic description of the framework, refer to Figure 7.

VI. EXPERIMENTS AND RESULTS

This section presents the numerical simulation of the proposed QGCNN on the task of classifying different HEP events. The input data are in the dimension of 32×32 . As noted, the dataset used in this study is the same as the one used in the previous work [32] (to aid comparison). The minor difference is that in this work, the image is padded into 32×32 for the amplitude encoding, which requires an input vector with a dimension of 2^n .

Here, we compare our hybrid quantum-classical graph convolution models with three other related models (Table I). We set the MLP as the baseline in this work. We also compare to results reported on the same dataset from previous work using QCNN and

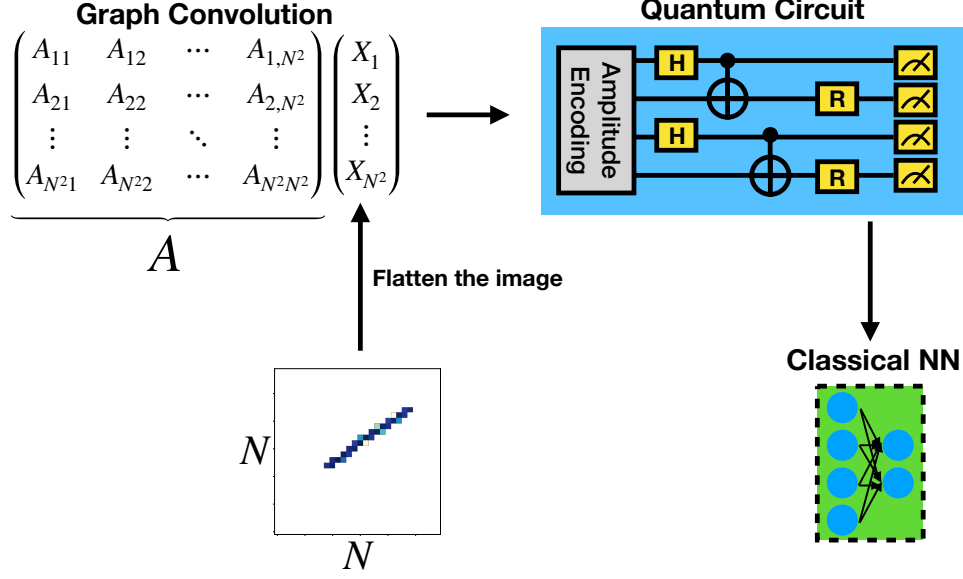


FIG. 7. **Hybrid Quantum-Classical Graph Convolution.** The proposed hybrid quantum-classical graph CNN contains three major components: 1) graph convolution 2) VQC, and 3) classical post-processing. The input image with dimension $N \times N$ will be operated first by the matrix A . Then, the processed input is encoded into a quantum state via amplitude encoding. Depending on the problem of interest, the quantum circuit portion may contain several different VQC blocks. The quantum measurement values from the final VQC block will be processed by a classical unit, which can be a neural network, to generate the logits of each class for classification.

classical CNN with a similar number of parameters [32].

| | QGCNN | MLP | QCNN ^a | CNN ^a |
|----------------------|-------|--------|-------------------|------------------|
| Number of Parameters | 202 | 131458 | 472 | 498 |

^a QCNN and CNN are from the work [32].

TABLE I. **Comparison of the number of parameters in different models.** The proposed QGCNN is compared with other related architectures in terms of the number of parameters. The MLP is the baseline used in this work with a single hidden layer. The QCNN and CNN are from the previous work [32].

For the proposed QGCNN, we first process the input image X with the adjacency matrix A . The transformed input A^2X then is encoded into the quantum circuit via amplitude encoding. There are two VQC blocks in the model, separated by a quantum measurement

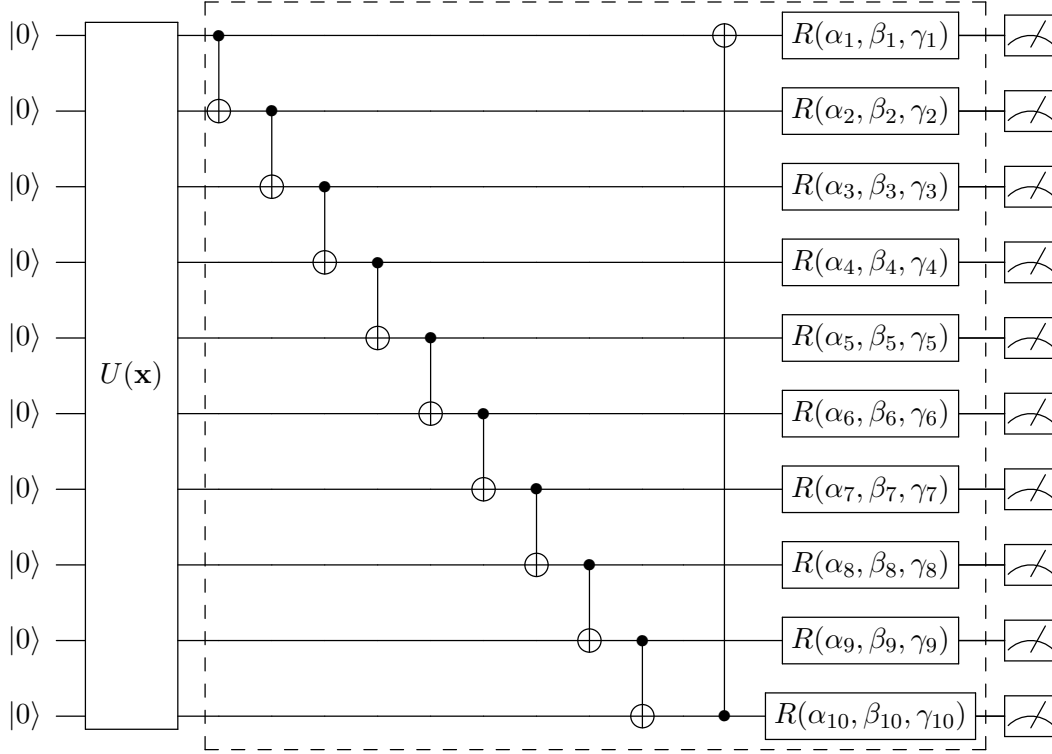


FIG. 8. **Variational quantum circuit architecture for the classifier with amplitude encoding.** The first VQC block encodes the vector after the graph convolution operation. The N -dimensional vector is encoded via amplitude encoding into a $\log(N)$ -qubit state. In this work, $N = 10$. The $U(\mathbf{x})$ is the quantum routine for amplitude encoding, which is described in [62, 64]. The parameters labeled with α_i , β_i , and γ_i are for optimization. The grouped box in the circuit may repeat several times to increase the number of parameters, subject to the capacity and capability of the available quantum devices or simulation software used for the experiments. The number of repeat is a hyperparameter and should be chosen carefully. In this work, the number of repeat is set to be 3.

layer. The first quantum circuit block (shown in Figure 8) is in conjunction with the amplitude encoding routine and has $10 \times 3 \times 3 = 90$ parameters. The second quantum block (shown in Figure 9) encodes the measured values from the first block then operates on another $10 \times 3 \times 3 = 90$ parameters. The measured expectation values from the second block are processed with a single-layer classical neural network (with $10 \times 2 + 2 = 22$ parameters) to output two-dimensional logits for binary classification. Therefore, the total number of parameters in the QGCNN model is $90 + 90 + 22 = 202$. The MLP baseline used in this

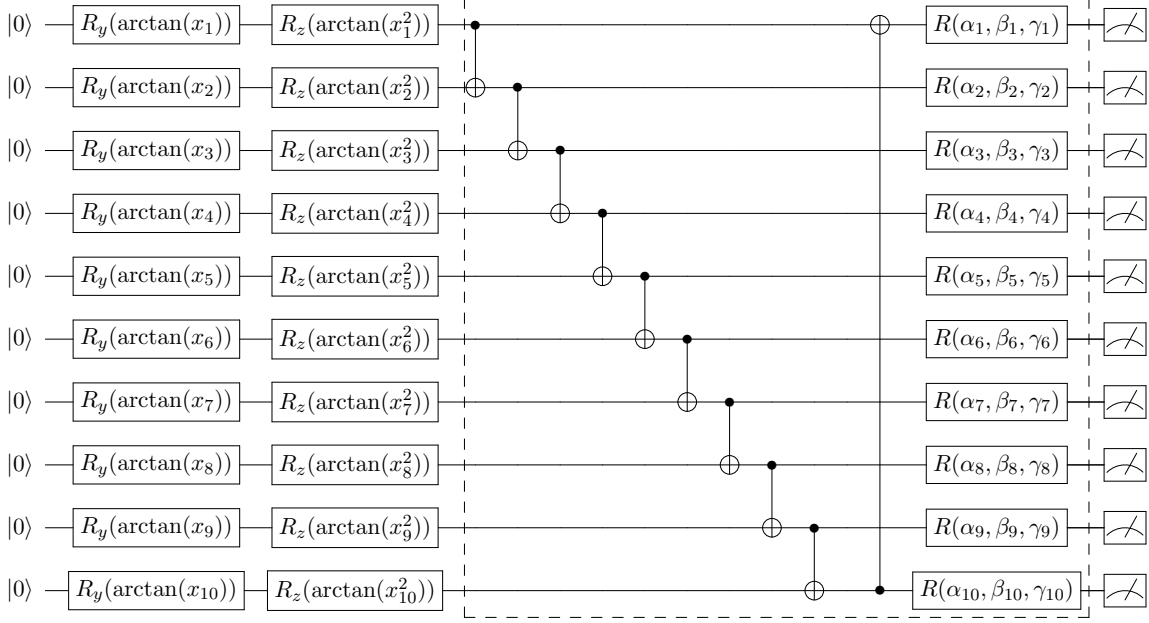


FIG. 9. **Variational quantum circuit block with variational encoding.** This encoding part includes R_y and R_z rotations, parameterized by the rotation angles $\arctan(x_i)$ and $\arctan(x_i^2)$ for each qubit. The parameters labeled with α_i , β_i , and γ_i are for optimization. The grouped box in the circuit may repeat several times to increase the number of parameters, subject to the capacity and capability of the available quantum devices or simulation software used for the experiments. The number of repeat is a hyperparameter and should be chosen carefully. In this work, the number of repeat is set to be 3.

work is: $1024 \times 128 + 128 + 128 \times 2 + 2 = 131458$. The software used for this work includes PyTorch [69], PennyLane [66], and Qulacs [70].

A. Muon versus Electron

Figure 11 and Table II show the results of the classification between μ^+ and e^- . A μ^+ is a track-like particle, while an e^- produces electromagnetic showers that are spatially extended. The patterns from these two particles are rather distinctive visually. For better comparison, we include the QCNN and CNN from the previous work [32]. In this experiment, we can observe comparable performance in the four different architectures in terms of testing accuracies. While QGCNN has a slightly better testing accuracy, the margin is not significant because this particular task is not too difficult. If we consider the number of parameters, it

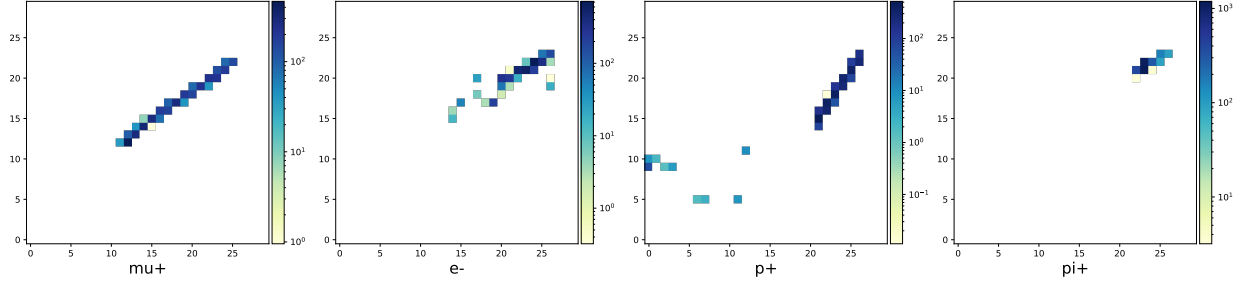


FIG. 10. Examples of scaled images of simulated particle activities (μ^+ , π^+ , p , e^-) in a LArTPC detector. These are the images used in the QGCNN experiments. In the experiment, we pad 0 to the image, so the dimension of these images is 32×32 , which is for amplitude encoding with a 10-qubit quantum circuit.

is evident that QGCNN performs better as it requires fewer model parameters.

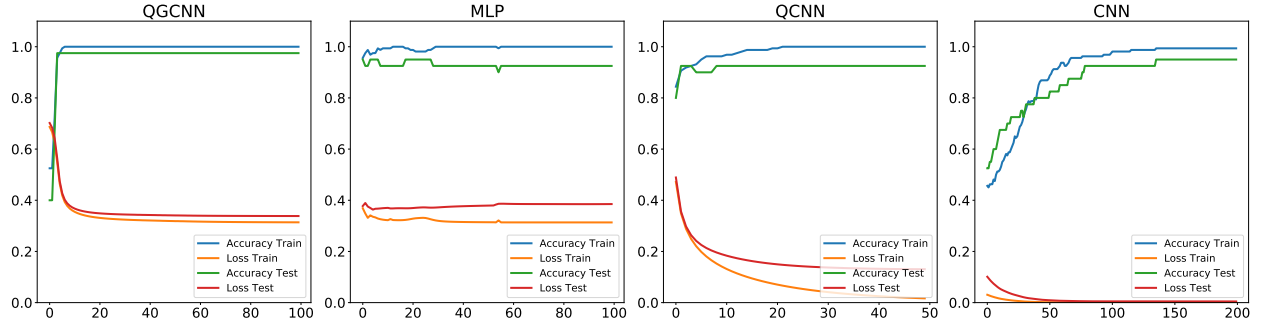


FIG. 11. **Result: Hybrid Quantum-Classical GCN on binary classification of muon versus electron.** Comparison of performance between different architectures in the task of binary classification of muon versus electron. For a better comparison, results from the previous work on QCNN versus CNN are included [32]. In Table I, we present the number of parameters in differing architectures.

B. Muon versus Proton

Figure 12 and Table III show the results of the classification between μ^+ and p . Because a proton's mass is much heavier than a muon, it has higher energy deposition per unit length and encounters less multiple Coulomb scattering when it passes the detector. As a result, a proton's track has higher pixel intensity and is straighter than that of a muon. Here,

| | Training Accuracy | Testing Accuracy | Training Loss | Testing Loss |
|-------------------|-------------------|------------------|---------------|--------------|
| QGCNN | 100% | 97.5% | 0.3138 | 0.3384 |
| MLP | 100% | 92.5% | 0.3134 | 0.3852 |
| QCNN ^a | 100% | 92.5% | 0.017 | 0.13 |
| CNN ^a | 99.38% | 95% | 0.0002 | 0.0046 |

^a QCNN and CNN are from the work [32].

TABLE II. Performance comparison between QGCNN and other QML architectures on the binary classification between μ^+ versus e^- .

we include the QCNN and CNN from the previous work [32] for better comparison. In this experiment, QGCNN presents a comparable performance to QCNN in terms of testing accuracies. However, QGCNN requires fewer parameters than QCNN. We also observe that QGCNN has significantly better performance than the MLP baseline and CNN. Specifically, the number of parameters in QGCNN is much lower than that of the MLP.

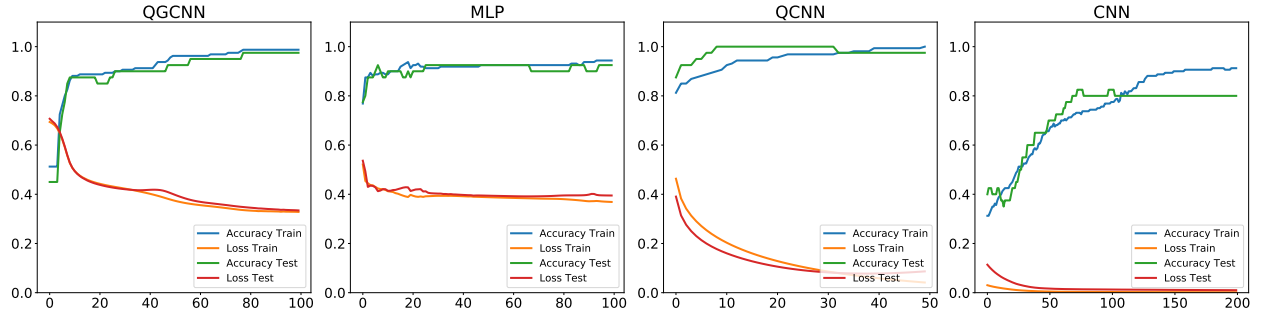


FIG. 12. **Result: Hybrid Quantum-Classical GCN on binary classification of muon versus proton.** Comparison of performance between different architectures in the task of muon versus proton binary classification. Results from the previous work with QCNN versus CNN are included for better comparison [32]. Table I also presents the number of parameters in differing architectures.

C. Muon versus Charged Pion

Figure 13 and Table IV depict the results of the classification between μ^+ and π^+ . A charged pion behaves similarly to a muon because their masses are closer. The main dif-

| | Training Accuracy | Testing Accuracy | Training Loss | Testing Loss |
|-------------------|-------------------|------------------|---------------|--------------|
| QGCNN | 98.75% | 97.5% | 0.3283 | 0.3344 |
| MLP | 94.38% | 92.5% | 0.3688 | 0.3950 |
| QCNN ^a | 100.00% | 97.5% | 0.041 | 0.087 |
| CNN ^a | 91.25% | 80% | 0.002 | 0.01 |

^a QCNN and CNN are from the work [32].

TABLE III. Performance comparison between QGCNN and other QML architectures on the binary classification between μ^+ versus p .

ference is that the π^+ experiences additional nuclear interactions during its passage in the detector, often leading to a large-angle “kink” along its main trajectory. For better comparison, we include the QCNN and CNN from the previous work [32]. In this experiment, QGCNN illustrates a comparable performance to QCNN in terms of testing accuracies. However, QGCNN requires fewer parameters than QCNN. We also observe that QGCNN offers significantly better performance than the MLP baseline and CNN. In particular, the number of parameters in QGCNN is much lower than that of MLP.

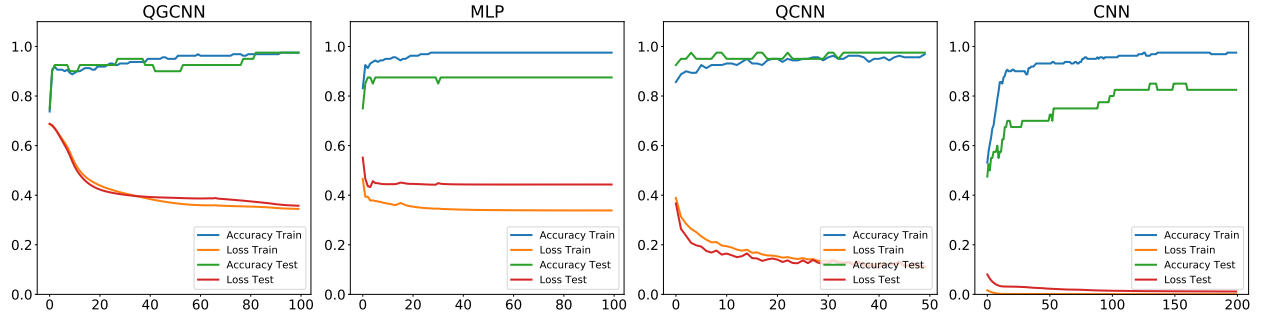


FIG. 13. **Result: Hybrid Quantum-Classical GCN on binary classification of muon versus charged pion.** Comparison of performance between different architectures in the task of muon versus charged pion binary classification. Results from the previous work on QCNN versus CNN are included for better comparison [32]. Table I also presents the number of parameters in differing architectures.

| | Training Accuracy | Testing Accuracy | Training Loss | Testing Loss |
|-------------------|-------------------|------------------|---------------|--------------|
| QGCNN | 97.5% | 97.5% | 0.3448 | 0.3574 |
| MLP | 97.5% | 87.5% | 0.3384 | 0.4431 |
| QCNN ^a | 96.88% | 97.5% | 0.1066 | 0.1121 |
| CNN ^a | 97.5% | 82.5% | 0.0006 | 0.0116 |

^a QCNN and CNN are from the work [32].

TABLE IV. Performance comparison between QGCNN and other QML architectures on the binary classification between μ^+ versus π^+ .

VII. DISCUSSION

A. Quantum Graph Encoding

In this work, we combine the classical aggregation matrix and quantum amplitude encoding to perform the classification. It is interesting to investigate the possibility of performing the graph convolution step with the quantum operation. For example, the work in [71] introduced a method of encoding the Laplacian eigenmap with VQC. In the work of [72], the authors propose a graph embedding method based on variational circuits to deal with knowledge graphs.

B. Future Applications

Graph CNNs have been studied extensively among the classical ML community [9–11, 73–76]. Several important applications have been demonstrated, for example, social network prediction [73, 77], traffic problems [78, 79], recommender systems [80, 81], graph representation [82], graph generation [83, 84], computational chemistry [85], drug development [75], and modeling physical dynamics [86] (to name a few). Our hybrid quantum-classical model is expected to be applicable to most of these aforementioned areas. Another interesting will be to investigate the potential quantum advantages of using different quantum architectures in diverse real-world scenarios.

C. Quantum Machine Learning in High Energy Physics

Applying QML in HEP data analysis is an emerging field, yet there are several related works in this area. These works [61, 87, 88] focus on event classification with QML models. For example, [61, 87] used similar VQC models to study the classification problems in HEP. However, the input dimension is limited. In [88], the authors used a quantum-inspired classical algorithms, called “tree tensor network,” to study the classification problem. The tensor network formulation has a direct corollary in the quantum circuit model. The underlying relationships of these models and other purely VQC-based models deserve further investigation. Recent advances in building more sophisticated QML models also have led to the successful demonstration of applying QCNN to HEP event classification [32]. Meanwhile, using classical graph neural networks in HEP research has become popular [89]. The work in [90] proposed a quantum graph model for particle track reconstruction. However, our approach differs from this one. We employ a classical graph convolutional operation on a regular graph that is an image then encode the transformed vector into a quantum state via amplitude encoding to reduce the number of qubits used. For more in-depth discussions regarding QML in HEP, refer to recent reviews [91, 92].

VIII. CONCLUSION

This work demonstrates a hybrid quantum classical QCNN that extends the power of graph convolution operation to enhance the features gleaned from input data and the capability of quantum superposition to greatly reduce the number of model parameters used. Notably, we numerically show the significantly superior performance in terms of testing accuracies over using classical MLP, classical CNN, and recent QCNN methods. These results indicate the potential benefits such capabilities can bring to the HEP community and other scientific areas in the quantum era.

ACKNOWLEDGMENTS

This work is supported by the U.S. Department of Energy, Office of Science, Office of High Energy Physics program under Award Number DE-SC-0012704 and Brookhaven National

- [1] P. Baldi, P. Sadowski, and D. Whiteson, "Searching for exotic particles in high-energy physics with deep learning," *Nature communications*, vol. 5, no. 1, pp. 1–9, 2014.
- [2] D. Guest, K. Cranmer, and D. Whiteson, "Deep learning and its application to lhc physics," *Annual Review of Nuclear and Particle Science*, vol. 68, pp. 161–181, 2018.
- [3] P. Baldi, K. Bauer, C. Eng, P. Sadowski, and D. Whiteson, "Jet substructure classification in high-energy physics with deep neural networks," *Physical Review D*, vol. 93, no. 9, p. 094034, 2016.
- [4] P. Baldi, K. Cranmer, T. Faucett, P. Sadowski, and D. Whiteson, "Parameterized neural networks for high-energy physics," *The European Physical Journal C*, vol. 76, no. 5, pp. 1–7, 2016.
- [5] D. Guest, J. Collado, P. Baldi, S.-C. Hsu, G. Urban, and D. Whiteson, "Jet flavor classification in high-energy physics with deep neural networks," *Physical Review D*, vol. 94, no. 11, p. 112002, 2016.
- [6] L. de Oliveira, M. Kagan, L. Mackey, B. Nachman, and A. Schwartzman, "Jet-images—deep learning edition," *Journal of High Energy Physics*, vol. 2016, no. 7, p. 69, 2016.
- [7] A. Aurisano, A. Radovic, D. Rocco, A. Himmel, M. Messier, E. Niner, G. Pawloski, F. Psihas, A. Sousa, and P. Vahle, "A convolutional neural network neutrino event classifier," *Journal of Instrumentation*, vol. 11, no. 09, p. P09001, 2016.
- [8] B. Abi, R. Acciarri, M. Acero, G. Adamov, D. Adams, M. Adinolfi, Z. Ahmad, J. Ahmed, T. Alion, S. A. Monsalve, *et al.*, "Neutrino interaction classification with a convolutional neural network in the dune far detector," *Physical Review D*, vol. 102, no. 9, p. 092003, 2020.
- [9] Z. Wu, S. Pan, F. Chen, G. Long, C. Zhang, and S. Y. Philip, "A comprehensive survey on graph neural networks," *IEEE Transactions on Neural Networks and Learning Systems*, 2020.
- [10] J. Zhou, G. Cui, Z. Zhang, C. Yang, Z. Liu, L. Wang, C. Li, and M. Sun, "Graph neural networks: A review of methods and applications," *arXiv preprint arXiv:1812.08434*, 2018.
- [11] S. Zhang, H. Tong, J. Xu, and R. Maciejewski, "Graph convolutional networks: Algorithms, applications and open challenges," in *International Conference on Computational Social Networks*, pp. 79–91, Springer, 2018.

- [12] F. Arute, K. Arya, R. Babbush, D. Bacon, J. C. Bardin, R. Barends, R. Biswas, S. Boixo, F. G. Brandao, D. A. Buell, *et al.*, “Quantum supremacy using a programmable superconducting processor,” *Nature*, vol. 574, no. 7779, pp. 505–510, 2019.
- [13] A. Cross, “The ibm q experience and qiskit open-source quantum computing software,” in *APS Meeting Abstracts*, 2018.
- [14] N. Grzesiak, R. Blümel, K. Wright, K. M. Beck, N. C. Pienti, M. Li, V. Chaplin, J. M. Amini, S. Debnath, J.-S. Chen, *et al.*, “Efficient arbitrary simultaneously entangling gates on a trapped-ion quantum computer,” *Nature Communications*, vol. 11, no. 1, pp. 1–6, 2020.
- [15] A. W. Harrow and A. Montanaro, “Quantum computational supremacy,” *Nature*, vol. 549, no. 7671, pp. 203–209, 2017.
- [16] M. A. Nielsen and I. Chuang, “Quantum computation and quantum information,” 2002.
- [17] P. W. Shor, “Polynomial-time algorithms for prime factorization and discrete logarithms on a quantum computer,” *SIAM review*, vol. 41, no. 2, pp. 303–332, 1999.
- [18] L. K. Grover, “Quantum mechanics helps in searching for a needle in a haystack,” *Physical review letters*, vol. 79, no. 2, p. 325, 1997.
- [19] J. Preskill, “Quantum computing in the nisc era and beyond,” *Quantum*, vol. 2, p. 79, 2018.
- [20] M. Cerezo, A. Arrasmith, R. Babbush, S. C. Benjamin, S. Endo, K. Fujii, J. R. McClean, K. Mitarai, X. Yuan, L. Cincio, *et al.*, “Variational quantum algorithms,” *arXiv preprint arXiv:2012.09265*, 2020.
- [21] A. Peruzzo, J. McClean, P. Shadbolt, M.-H. Yung, X.-Q. Zhou, P. J. Love, A. Aspuru-Guzik, and J. L. O’Brien, “A variational eigenvalue solver on a photonic quantum processor,” *Nature communications*, vol. 5, p. 4213, 2014.
- [22] M. Schuld, A. Bocharov, K. Svore, and N. Wiebe, “Circuit-centric quantum classifiers,” *arXiv preprint arXiv:1804.00633*, 2018.
- [23] E. Farhi and H. Neven, “Classification with quantum neural networks on near term processors,” *arXiv preprint arXiv:1802.06002*, 2018.
- [24] M. Benedetti, E. Lloyd, S. Sack, and M. Fiorentini, “Parameterized quantum circuits as machine learning models,” *Quantum Science and Technology*, vol. 4, no. 4, p. 043001, 2019.
- [25] A. Mari, T. R. Bromley, J. Izaac, M. Schuld, and N. Killoran, “Transfer learning in hybrid classical-quantum neural networks,” *arXiv preprint arXiv:1912.08278*, 2019.

- [26] Z. Abohashima, M. Elhosen, E. H. Houssein, and W. M. Mohamed, “Classification with quantum machine learning: A survey,” *arXiv preprint arXiv:2006.12270*, 2020.
- [27] P. Easom-McCaldin, A. Bouridane, A. Belatreche, and R. Jiang, “Towards building a facial identification system using quantum machine learning techniques,” *arXiv preprint arXiv:2008.12616*, 2020.
- [28] A. Sarma, R. Chatterjee, K. Gili, and T. Yu, “Quantum unsupervised and supervised learning on superconducting processors,” *arXiv preprint arXiv:1909.04226*, 2019.
- [29] S. Y.-C. Chen, C.-M. Huang, C.-W. Hsing, and Y.-J. Kao, “Hybrid quantum-classical classifier based on tensor network and variational quantum circuit,” *arXiv preprint arXiv:2011.14651*, 2020.
- [30] S. A. Stein, B. Baheri, R. M. Tischio, Y. Chen, Y. Mao, Q. Guan, A. Li, and B. Fang, “A hybrid system for learning classical data in quantum states,” *arXiv preprint arXiv:2012.00256*, 2020.
- [31] S. Y.-C. Chen, S. Yoo, and Y.-L. L. Fang, “Quantum long short-term memory,” *arXiv preprint arXiv:2009.01783*, 2020.
- [32] S. Y.-C. Chen, T.-C. Wei, C. Zhang, H. Yu, and S. Yoo, “Quantum convolutional neural networks for high energy physics data analysis,” *arXiv preprint arXiv:2012.12177*, 2020.
- [33] O. Kyriienko, A. E. Paine, and V. E. Elfving, “Solving nonlinear differential equations with differentiable quantum circuits,” *arXiv preprint arXiv:2011.10395*, 2020.
- [34] P.-L. Dallaire-Demers and N. Killoran, “Quantum generative adversarial networks,” *Physical Review A*, vol. 98, no. 1, p. 012324, 2018.
- [35] S. A. Stein, B. Baheri, R. M. Tischio, Y. Mao, Q. Guan, A. Li, B. Fang, and S. Xu, “Qugan: A generative adversarial network through quantum states,” *arXiv preprint arXiv:2010.09036*, 2020.
- [36] C. Zoufal, A. Lucchi, and S. Woerner, “Quantum generative adversarial networks for learning and loading random distributions,” *npj Quantum Information*, vol. 5, no. 1, pp. 1–9, 2019.
- [37] H. Situ, Z. He, L. Li, and S. Zheng, “Quantum generative adversarial network for generating discrete data,” *arXiv preprint arXiv:1807.01235*, 2018.
- [38] K. Nakaji and N. Yamamoto, “Quantum semi-supervised generative adversarial network for enhanced data classification,” *arXiv preprint arXiv:2010.13727*, 2020.

- [39] S. Lloyd, M. Schuld, A. Ijaz, J. Izaac, and N. Killoran, “Quantum embeddings for machine learning,” *arXiv preprint arXiv:2001.03622*, 2020.
- [40] N. A. Nghiem, S. Y.-C. Chen, and T.-C. Wei, “A unified classification framework with quantum metric learning,” *arXiv preprint arXiv:2010.13186*, 2020.
- [41] S. Y.-C. Chen, C.-H. H. Yang, J. Qi, P.-Y. Chen, X. Ma, and H.-S. Goan, “Variational quantum circuits for deep reinforcement learning,” *IEEE Access*, vol. 8, pp. 141007–141024, 2020.
- [42] O. Lockwood and M. Si, “Reinforcement learning with quantum variational circuit,” in *Proceedings of the AAAI Conference on Artificial Intelligence and Interactive Digital Entertainment*, vol. 16, pp. 245–251, 2020.
- [43] S. Wu, S. Jin, D. Wen, and X. Wang, “Quantum reinforcement learning in continuous action space,” *arXiv preprint arXiv:2012.10711*, 2020.
- [44] S. Jerbi, L. M. Trenkwalder, H. P. Nautrup, H. J. Briegel, and V. Dunjko, “Quantum enhancements for deep reinforcement learning in large spaces,” *arXiv preprint arXiv:1910.12760*, 2019.
- [45] C.-C. CHEN, K. SHIBA, M. SOGABE, K. SAKAMOTO, and T. SOGABE, “Hybrid quantum-classical ulam-von neumann linear solver-based quantum dynamic programming algorithm,” *Proceedings of the Annual Conference of JSAI*, vol. JS�2020, pp. 2K6ES203–2K6ES203, 2020.
- [46] J. Bausch, “Recurrent quantum neural networks,” *arXiv preprint arXiv:2006.14619*, 2020.
- [47] C.-H. H. Yang, J. Qi, S. Y.-C. Chen, P.-Y. Chen, S. M. Siniscalchi, X. Ma, and C.-H. Lee, “Decentralizing feature extraction with quantum convolutional neural network for automatic speech recognition,” *arXiv preprint arXiv:2010.13309*, 2020.
- [48] B. Abi *et al.*, “Deep Underground Neutrino Experiment (DUNE), Far Detector Technical Design Report, Volume II DUNE Physics,” 2 2020.
- [49] B. Viren *et al.*, “Wire-Cell Toolkit.” <https://github.com/WireCell/wire-cell-toolkit>, 2020.
- [50] E. L. Snider and G. Petrillo, “LArSoft: toolkit for simulation, reconstruction and analysis of liquid argon TPC neutrino detectors,” in *Journal of Physics Conference Series*, vol. 898 of *Journal of Physics Conference Series*, p. 042057, Oct. 2017.
- [51] C. Rubbia, “The Liquid Argon Time Projection Chamber: A New Concept for Neutrino Detectors,” *CERN-EP-INT-77-08, CERN-EP-77-08*, 5 1977.

- [52] H. H. Chen, P. E. Condon, B. C. Barish, and F. J. Sciulli, “A Neutrino detector sensitive to rare processes. I. A Study of neutrino electron reactions,” *FERMILAB-PROPOSAL-0496*, 1976.
- [53] W. Willis and V. Radeka, “Liquid Argon Ionization Chambers as Total Absorption Detectors,” *Nucl. Instrum. Meth.*, vol. 120, pp. 221–236, 1974.
- [54] D. Nygren, “The Time Projection Chamber: A New 4 pi Detector for Charged Particles,” *eConf*, vol. C740805, p. 58, 1974.
- [55] C. Adams *et al.*, “Ionization electron signal processing in single phase LArTPCs. Part I. Algorithm Description and quantitative evaluation with MicroBooNE simulation,” *JINST*, vol. 13, no. 07, p. P07006, 2018.
- [56] S. Sim, P. D. Johnson, and A. Aspuru-Guzik, “Expressibility and entangling capability of parameterized quantum circuits for hybrid quantum-classical algorithms,” *Advanced Quantum Technologies*, vol. 2, no. 12, p. 1900070, 2019.
- [57] T. Lanting, A. J. Przybysz, A. Y. Smirnov, F. M. Spedalieri, M. H. Amin, A. J. Berkley, R. Harris, F. Altomare, S. Boixo, P. Bunyk, *et al.*, “Entanglement in a quantum annealing processor,” *Physical Review X*, vol. 4, no. 2, p. 021041, 2014.
- [58] Y. Du, M.-H. Hsieh, T. Liu, and D. Tao, “The expressive power of parameterized quantum circuits,” *arXiv preprint arXiv:1810.11922*, 2018.
- [59] A. Abbas, D. Sutter, C. Zoufal, A. Lucchi, A. Figalli, and S. Woerner, “The power of quantum neural networks,” *arXiv preprint arXiv:2011.00027*, 2020.
- [60] K. Mitarai, M. Negoro, M. Kitagawa, and K. Fujii, “Quantum circuit learning,” *Physical Review A*, vol. 98, no. 3, p. 032309, 2018.
- [61] S. L. Wu, J. Chan, W. Guan, S. Sun, A. Wang, C. Zhou, M. Livny, F. Carminati, A. Di Meglio, A. C. Li, *et al.*, “Application of quantum machine learning using the quantum variational classifier method to high energy physics analysis at the lhc on ibm quantum computer simulator and hardware with 10 qubits,” *arXiv preprint arXiv:2012.11560*, 2020.
- [62] M. Schuld and F. Petruccione, “Information encoding,” in *Supervised Learning with Quantum Computers*, pp. 139–171, Cham: Springer International Publishing, 2018.
- [63] D. Sierra-Sosa, M. Telahun, and A. S. Elmaghraby, “Tensorflow quantum: Impacts of quantum state preparation on quantum machine learning performance,” *IEEE Access*, 2020.

- [64] M. Möttönen, J. J. Vartiainen, V. Bergholm, and M. M. Salomaa, “Transformation of quantum states using uniformly controlled rotations,” *Quant. Inf. Comp.*, vol. 5, no. 6, pp. 467–473, 2005.
- [65] M. Schuld, V. Bergholm, C. Gogolin, J. Izaac, and N. Killoran, “Evaluating analytic gradients on quantum hardware,” *Physical Review A*, vol. 99, no. 3, p. 032331, 2019.
- [66] V. Bergholm, J. Izaac, M. Schuld, C. Gogolin, C. Blank, K. McKiernan, and N. Killoran, “Pennylane: Automatic differentiation of hybrid quantum-classical computations,” *arXiv preprint arXiv:1811.04968*, 2018.
- [67] S. Ruder, “An overview of gradient descent optimization algorithms,” *arXiv preprint arXiv:1609.04747*, 2016.
- [68] T. Tieleman and G. Hinton, “Lecture 6.5—RmsProp: Divide the gradient by a running average of its recent magnitude.” COURSERA: Neural Networks for Machine Learning, 2012.
- [69] A. Paszke, S. Gross, F. Massa, A. Lerer, J. Bradbury, G. Chanan, T. Killeen, Z. Lin, N. Gimelshein, L. Antiga, *et al.*, “Pytorch: An imperative style, high-performance deep learning library,” in *Advances in neural information processing systems*, pp. 8026–8037, 2019.
- [70] Y. Suzuki, Y. Kawase, Y. Masumura, Y. Hiraga, M. Nakadai, J. Chen, K. M. Nakanishi, K. Mitarai, R. Imai, S. Tamiya, *et al.*, “Qulacs: a fast and versatile quantum circuit simulator for research purpose,” *arXiv preprint arXiv:2011.13524*, 2020.
- [71] S. Thabet and J.-F. Hullo, “Laplacian eigenmaps with variational circuits: a quantum embedding of graph data,” *arXiv preprint arXiv:2011.05128*, 2020.
- [72] Y. Ma, V. Tresp, L. Zhao, and Y. Wang, “Variational quantum circuit model for knowledge graph embedding,” *Advanced Quantum Technologies*, vol. 2, no. 7-8, p. 1800078, 2019.
- [73] T. N. Kipf and M. Welling, “Semi-supervised classification with graph convolutional networks,” *arXiv preprint arXiv:1609.02907*, 2016.
- [74] M. Henaff, J. Bruna, and Y. LeCun, “Deep convolutional networks on graph-structured data,” *arXiv preprint arXiv:1506.05163*, 2015.
- [75] M. Sun, S. Zhao, C. Gilvary, O. Elemento, J. Zhou, and F. Wang, “Graph convolutional networks for computational drug development and discovery,” *Briefings in bioinformatics*, vol. 21, no. 3, pp. 919–935, 2020.
- [76] S. Liu, J. H. Park, and S. Yoo, “Efficient and effective graph convolution networks,” in *Proceedings of the 2020 SIAM International Conference on Data Mining*, pp. 388–396, SIAM,

2020.

- [77] W. Hamilton, Z. Ying, and J. Leskovec, “Inductive representation learning on large graphs,” in *Advances in neural information processing systems*, pp. 1024–1034, 2017.
- [78] A. Rahimi, T. Cohn, and T. Baldwin, “Semi-supervised user geolocation via graph convolutional networks,” *arXiv preprint arXiv:1804.08049*, 2018.
- [79] Z. Cui, K. Henrickson, R. Ke, and Y. Wang, “Traffic graph convolutional recurrent neural network: A deep learning framework for network-scale traffic learning and forecasting,” *IEEE Transactions on Intelligent Transportation Systems*, 2019.
- [80] R. Ying, R. He, K. Chen, P. Eksombatchai, W. L. Hamilton, and J. Leskovec, “Graph convolutional neural networks for web-scale recommender systems,” in *Proceedings of the 24th ACM SIGKDD International Conference on Knowledge Discovery & Data Mining*, pp. 974–983, 2018.
- [81] R. v. d. Berg, T. N. Kipf, and M. Welling, “Graph convolutional matrix completion,” *arXiv preprint arXiv:1706.02263*, 2017.
- [82] Z. Ying, J. You, C. Morris, X. Ren, W. Hamilton, and J. Leskovec, “Hierarchical graph representation learning with differentiable pooling,” in *Advances in neural information processing systems*, pp. 4800–4810, 2018.
- [83] A. Bojchevski, O. Shchur, D. Zügner, and S. Günnemann, “Netgan: Generating graphs via random walks,” *arXiv preprint arXiv:1803.00816*, 2018.
- [84] J. You, B. Liu, Z. Ying, V. Pande, and J. Leskovec, “Graph convolutional policy network for goal-directed molecular graph generation,” in *Advances in neural information processing systems*, pp. 6410–6421, 2018.
- [85] D. K. Duvenaud, D. Maclaurin, J. Iparraguirre, R. Bombarell, T. Hirzel, A. Aspuru-Guzik, and R. P. Adams, “Convolutional networks on graphs for learning molecular fingerprints,” *Advances in neural information processing systems*, vol. 28, pp. 2224–2232, 2015.
- [86] P. W. Battaglia, R. Pascanu, M. Lai, D. Rezende, and K. Kavukcuoglu, “Interaction networks for learning about objects, relations and physics,” *arXiv preprint arXiv:1612.00222*, 2016.
- [87] K. Terashi, M. Kaneda, T. Kishimoto, M. Saito, R. Sawada, and J. Tanaka, “Event classification with quantum machine learning in high-energy physics,” *arXiv preprint arXiv:2002.09935*, 2020.

- [88] M. Trenti, L. Sestini, A. Gianelle, D. Zuliani, T. Felser, D. Lucchesi, and S. Montanero, “Quantum-inspired machine learning on high-energy physics data,” *arXiv preprint arXiv:2004.13747*, 2020.
- [89] J. Shlomi, P. Battaglia, *et al.*, “Graph neural networks in particle physics,” *Machine Learning: Science and Technology*, 2020.
- [90] C. Tüysüz, F. Carminati, B. Demirköz, D. Dobos, F. Fracas, K. Novotny, K. Potamianos, S. Vallecorsa, and J.-R. Vlimant, “A quantum graph neural network approach to particle track reconstruction,” *arXiv preprint arXiv:2007.06868*, 2020.
- [91] W. Guan, G. Perdue, A. Pesah, M. Schuld, K. Terashi, S. Vallecorsa, and J.-R. Vlimant, “Quantum machine learning in high energy physics,” *arXiv preprint arXiv:2005.08582*, 2020.
- [92] K. K. Sharma, “Quantum machine learning and its supremacy in high energy physics,” *Modern Physics Letters A*, p. 2030024, 2020.